

ROTATIONAL SPLITTING AND ASTEROSEISMIC MODELLING OF THE δ SCUTI STAR EE CAMELOPARDALIS

XINGHAO CHEN^{1,2,3} AND YAN LI^{1,2,3,4}
Draft version August 27, 2018

ABSTRACT

According to the rotational splitting law of g modes, the frequency spectra of EE Cam can be disentangled only with oscillation modes of $\ell = 0, 1$, and 2. Fifteen sets of rotational splits are found, containing five sets of $\ell = 1$ multiplets and ten sets of $\ell = 2$ multiplets. The rotational period of EE Cam is deduced to be $P_{\text{rot}} = 1.84_{-0.05}^{+0.07}$ days. When we do model fittings, we use two nonradial oscillation modes (f_{11} and f_{32}) and the fundamental radial mode f_1 . The fitting results show that χ^2 of the best-fitting model is much smaller than those of other theoretical models. The physical parameters of the best-fitting model are $M = 2.04 M_{\odot}$, $Z = 0.028$, $T_{\text{eff}} = 6433$ K, $\log L/L_{\odot} = 1.416$, $R = 4.12 R_{\odot}$, $\log g = 3.518$, and $\chi^2 = 0.00035$. Furthermore, we find f_{11} and f_{32} are mixed mode, which mainly characterize the features of the helium core. The fundamental radial mode f_1 mainly restrict the features of the stellar envelope. Finally, the acoustic radius τ_0 and the period separation Π_0 are determined to be 5.80 hr and 463.7 s respectively, and the size of the helium core of EE Cam is estimated to be $M_{\text{He}} = 0.181 M_{\odot}$ and $R_{\text{He}} = 0.0796 R_{\odot}$.

Subject headings: asteroseismology - stars: rotation - stars: individual: EE Cam - stars: variables: delta Scuti

1. INTRODUCTION

The δ Scuti pulsator EE Cam is classified as an F3 star on basis of the Strömngren indices (Olsen 1980). The star was firstly discovered to be a variable star in the *Hipparcos* mission (Perryman et al. 1997). Koen (2001) reanalyzed the *Hipparcos* epoch photometric data and obtained two frequencies of 4.93 cd^{-1} and 5.21 cd^{-1} . The first comprehensive frequency analysis of the photometric data for EE Cam was published by Breger et al. (2007). EE Cam was observed photometrically for 87 nights from 2006 to 2007 using the Vienna University Automatic Photoelectric Telescope (Strassmeier et al. 1997; Breger & Hiesberger 1999; Granzer et al. 2001), situated in Washington Camp, Arizona, USA. Fifteen oscillation frequencies were detected (Breger et al. 2007). With 213+ nights additional photometric data, the number of detected frequencies was increased to forty, of which thirty-seven were independent (Breger et al. 2015). These oscillation frequencies are shown in Table 1 of Breger et al. (2015).

In addition, Breger et al. (2015) compared the observed phase shifts and amplitude ratios with those derived from theoretical models. They identified the dominant mode $f_1 = 57.101 \mu\text{Hz}$ as a radial mode and the second dominant mode $f_2 = 60.345 \mu\text{Hz}$ as a nonradial mode with $\ell = 1$. Moreover, Breger et al. (2015) performed a detailed analysis of pulsation instability, and suggested the radial mode f_1 as the fundamental radial mode. Both of the radial mode and nonradial oscillation modes are detected. Different oscillation modes show different propagation behaviors in the star, thus EE Cam is an ideal object for asteroseismology.

Our work extends the work of Breger et al. (2015), and presents a comprehensive asteroseismic analysis for EE Cam. The present work is organized as follows. In Section 2, we

propose our mode identification on basis of rotational splitting. In Section 3, we describe the details of stellar models. Fundamental parameters of EE Cam is introduced in Section 3.1, Input physics are elaborated in Section 3.2, and model grids are presented in Section 3.3. We analyze our asteroseismic results in Section 4. The best-fitting model are elaborated in Section 4.1, the fitting result is discussed in Section 4.2. Finally, we conclude the results of our work in Section 5.

2. MODE IDENTIFICATIONS BASED ON THE ROTATIONAL SPLITTING

According to the theory of stellar oscillations, each oscillation mode can be characterized by three spherical harmonic numbers: the radial orders n , the spherical harmonic degree ℓ , and the azimuthal order m . If a star is rotating, departures from spherical symmetry caused by stellar rotation will result in the nonradial oscillation mode splitting into $2\ell+1$ different frequencies. For high-order g modes, the approximate formula of the rotational splitting $\delta\nu_{\ell,n}$ and the rotational period P_{rot} can be described as

$$\nu_{\ell,n,m} - \nu_{\ell,n,0} = m\delta\nu_{\ell,n} = \frac{m}{P_{\text{rot}}} \left(1 - \frac{1}{\ell(\ell+1)}\right) \quad (1)$$

(Brickhill 1975). In Equation (1), m varies from $-\ell$ to ℓ , a total of $2\ell+1$ different values. The value of $v \sin i$ of EE Cam is measured to be $40 \pm 3 \text{ km s}^{-1}$ by Breger et al. (2007) and to be $51 \pm 8 \text{ km s}^{-1}$ by Bush & Hintz (2008). The two results of $v \sin i$ are consistent within 1σ error. Besides, Breger et al. (2015) showed the inclination angle i being 34 ± 4 deg. Then the equatorial rotation velocity is estimated to be $72 \pm 10 \text{ km s}^{-1}$ from $v \sin i$ of Breger et al. (2007), and to be $91 \pm 25 \text{ km s}^{-1}$ from the result of Bush & Hintz (2008). According to the analyses of Chen et al. (2017), the second-order effect of rotation is much smaller than that of the first-order. Thus the second-order effect of rotation is neglected in our work.

According to Equation (1), splitting frequencies with $\ell = 1$ form a triplet and splitting frequencies with $\ell = 2$ form a quintuplet. Moreover, the rotational splitting of $\ell = 1$ modes

¹ Yunnan Observatories, Chinese Academy of Sciences, P.O. Box 110, Kunming 650011, PR China; chenxinghao@ynao.ac.cn; ly@ynao.ac.cn

² Key Laboratory for Structure and Evolution of Celestial Objects, Chinese Academy of Sciences, P.O. Box 110, Kunming 650011, PR China

³ University of Chinese Academy of Sciences, Beijing 100049, PR China

⁴ Center for Astronomical Mega-Science, Chinese Academy of Sciences, 20A Datun Road, Chaoyang District, Beijing, 100012, PR China

and that of $\ell = 2$ modes meet the proportional relation

$$\frac{\delta\nu_{\ell=1,n}}{\delta\nu_{\ell=2,n}} = 0.6 \quad (2)$$

(Winget et al. 1991). Based on the above analyses, we search for potentially rotational splits in the frequency spectra of EE Cam and list them in Table 1. The frequency ID in Table 1 follows the serial numbers of Breger et al. (2015).

A total of fifteen sets of possible multiplets are found. The averaged value of the frequency splitting $\delta\nu_1$ in Multiplet 1, 2, 3, 4, and 5 is $3.256 \mu\text{Hz}$. The averaged value of the frequency splitting $\delta\nu_2$ in Multiplet 6, 7, 8, 9, 10, 11, 12, 13, 14, and 15 is $5.403 \mu\text{Hz}$. The ratio of $\delta\nu_1$ and $\delta\nu_2$ is 0.603, which agrees well with Equation (2). We hence identify the spherical harmonic degree of frequencies in Multiplet 1, 2, 3, 4, and 5 as $\ell = 1$, and the spherical harmonic degree of frequencies in Multiplet 6, 7, 8, 9, 10, 11, 12, 13, 14, and 15 as $\ell = 2$. Furthermore, it can be noticed in Table 1 that the identifications of the azimuthal order m of oscillation frequencies are unique in Multiplet 1, 5, 6, 7, 13, 14, and 15. However, the identifications of the azimuthal order m of oscillation frequencies in other multiplets allow of more possibilities (e.g., two possibilities in Multiplet 2, 3, 4, 11, and 12, three possibilities in Multiplet 10, and four possibilities in Multiplet 8 and 9). The photometric mode identifications of Breger et al. (2015) show that f_2 is a mode with $\ell = 1$ and f_3 is a mode with $\ell = 1$ or $\ell = 2$. Moreover, Breger et al. (2015) suggest f_3 being a dipole mode on basis of the line-profile variations. Our mode identifications are in good agreement with those of Breger et al. (2015).

Finally, three oscillation frequencies do not show frequency splitting, i.e., f_{12} , f_{13} , and f_{23} . We notice that f_{12} and f_{28} have a frequency difference about $10.644 \mu\text{Hz}$, about twice of $\delta\nu_2$. However, f_{28} , f_{25} , and f_{11} has been identified as one complete triplet. The frequency difference between f_{28} and f_{11} is in good agreement with the value between f_{25} and f_{11} . The frequency difference between f_{23} and f_{25} is about $16.191 \mu\text{Hz}$, about three times of $\delta\nu_2$. The case of f_{23} is similar to that of f_{12} . The mode identification of f_{15} allows of two possibilities, i.e., as a mode with $\ell = 1$ or as a mode with $\ell = 2$. Frequencies f_5 and f_{15} have a difference of about $6.438 \mu\text{Hz}$, about twice of $\delta\nu_1$. Thus the spherical harmonic degree ℓ of f_5 and f_{15} can be identified as $\ell = 1$, and their azimuthal order m can be uniquely identified as being $m = (-1, +1)$. This case is listed in Table 1. Besides, f_{13} and f_{15} have a frequency difference of $21.689 \mu\text{Hz}$, about four times of $\delta\nu_2$. In this case, the spherical harmonic degree of f_{13} and f_{15} are identified as $\ell = 2$, and their azimuthal order m are uniquely identified as being $m = (-2, +2)$.

Based on the regularities of rotational splitting, five sets of multiplets with $\ell = 1$ and ten sets of multiplets with $\ell = 2$ are identified. Due to departures from the asymptotic formula, frequency differences in these multiplets may slightly deviate from the averaged values of rotational splitting. Furthermore, it can be noticed in Table 1 that only two components are detected in Multiplet 2, 3, 4, 5, 8, 9, 10, 11, 12, 13, 14, and 15. Other physical factors like the phenomenon of avoided crossings (Aizenman et al. 1977) and the large separation resulted from the isolated modes (García Hernández et al. 2013; Lignières et al. 2006) are also possible.

Based on above analyses, the frequency spectra of EE Cam can be disentangled only with oscillation modes of $\ell = 0, 1$, and 2. Oscillation modes with $\ell = 3$ are not considered in this

work. This situation is very different from those of HD 50844 (Chen et al. 2016) and CoRoT 102749568 (Chen et al. 2017). According to the theory of stellar oscillations, the spherical harmonic degree ℓ is the number of nodal lines by which the stellar surface is divided to oscillate in the opposite phase. The stellar surface will be divided into more zones for higher value of the spherical harmonic degree ℓ . Due to the effect of geometrical cancellation, the detections of oscillation frequencies with higher degree need much higher precision observations. The oscillation frequencies of HD 50844 (Poretti et al. 2009; Balona 2014) and CoRoT 102749568 (Paparó et al. 2013) are obtained from the CoRoT timeseries. However, the oscillation frequencies of EE Cam are extracted from the ground-based observations (Breger et al. 2015). Therefore, only oscillation modes with $\ell = 0, 1$, and 2 are considered in this work.

3. STELLAR MODELS

3.1. Fundamental parameters of EE Cam

The effective temperature T_{eff} of EE Cam is $T_{\text{eff}} = 6469_{-73}^{+65}$ K and the [Fe/H] abundance is $[\text{Fe}/\text{H}] = 0.24_{-0.13}^{+0.12}$ dex according to the catalog by Ammons et al. (2006). Based on the *Hipparcos* parallax 4.34 ± 0.63 mas of van Leeuwen et al. (2007), Breger et al. (2015) estimated the luminosity of EE Cam to be $\log L/L_{\odot} = 1.53_{-0.12}^{+0.14}$. The catalog of Nordström et al. (2014) shows values of T_{eff} and [Fe/H] being 6530 K and 0.06 respectively. In our work, we adopt a higher uncertainty of 200 K (e.g., Breger et al. 2015) for the effective temperature T_{eff} of Ammons et al. (2006). Meanwhile, we use a large range for the value of [Fe/H], varying from 0 to 0.36 dex, to cover the results of Nordström et al. (2004) and Ammons et al. (2006).

3.2. Input physics

We compute our theoretical models with the Modules for Experiments in Stellar Astrophysics (MESA; Paxton et al. 2011, 2013). The submodule "pulse" of version 6596 is used to compute stellar evolutionary models and to compute their corresponding oscillation frequencies (Christensen-Dalsgaard 2008; Paxton et al. 2011, 2013). Our theoretical models are constructed on basis of the OPAL opacity table GS98 (Grevesse & Sauval 1998) series. The Eddington grey atmosphere $T - \tau$ relation in the atmosphere integration is used. The mixing-length theory (MLT) of Böhm-Vitense (1958) is chosen to treat convection. Effects of element diffusion, convective overshooting, and rotation are not included in our calculations.

3.3. Model grids

In our calculations, we fix the mixing-length parameter α to the solar value of 1.80, and set the initial helium fraction $Y = 0.245 + 1.54Z$ (e.g., Dotter et al. 2008; Thompson et al. 2014), as a function of the metallicity Z . The value of Z varies from 0.015 to 0.035 with a step of 0.001. The stellar mass M varies from $1.5M_{\odot}$ to $2.5M_{\odot}$ with a step of $0.01M_{\odot}$.

Figure 1 illustrates the evolutionary tracks of the theoretical models on the Hertzsprung-Russell Diagram. In this figure, the rectangle marks the 1σ error box of the effective temperature T_{eff} and the luminosity $\log L/L_{\odot}$, i.e., $6269 \text{ K} < T_{\text{eff}} < 6669 \text{ K}$ and $1.41 < \log L/L_{\odot} < 1.67$. We calculate frequencies of oscillation modes with $\ell = 0, 1$, and 2 for every

stellar model falling inside the error box, and fitting them to the observed frequencies according to

$$\chi^2 = \frac{1}{k} \sum (|\nu_i^{\text{theo}} - \nu_i^{\text{obs}}|^2). \quad (3)$$

In Equation (3), ν_i^{theo} denotes the theoretical frequency, ν_i^{obs} denotes the observed frequency, and k denotes the number of the observed frequencies.

4. ASTEROSEISMIC ANALYSIS

4.1. The best-fitting model for EE Cam

In Section 2, we identify the observed frequencies based on the regularities of rotational splitting. In particular for the oscillation frequencies (f_{25}, f_{11}, f_{28}) in Multiplet 1 and (f_{10}, f_{32}, f_{37}) in Multiplet 6, mode identifications are unique and their $m = 0$ components are detected. When we do model fittings, we only use the two central components f_{11} , and f_{32} , as well as the the fundamental radial mode f_1 . Breger et al. (2015) identified f_1 as a radial mode based on the analyses of theoretical phase differences and amplitude ratios, and suggested f_1 as the fundamental radial mode based on a detailed analysis of pulsation instability. We use the identification of f_1 as the fundamental radial mode in our calculations.

In Figure 2, we illustrate the changes of $1/\chi^2$ as a function of the effective temperature T_{eff} for grid models. Each curve in Figure 2 corresponds to one evolutionary track in Figure 1. It can be clearly noticed that $1/\chi^2$ of the theoretical model with $Z=0.028$ and $M = 2.04M_{\odot}$ is much larger than those of other theoretical models. We hence choose the model with the minimum value of $\chi^2 = 0.00035$ as the best-fitting model, and mark it with a filled circle in Figure 2. The fundamental parameters of the best-fitting model are $M = 2.04 M_{\odot}$, $Z = 0.028$, $T_{\text{eff}} = 6433$ K, $\log L/L_{\odot} = 1.416$, $R = 4.120 R_{\odot}$, $\log g = 3.518$.

Theoretical oscillation frequencies deduced from the best-fitting model are listed in Table 2, in which n_p is the number of radial nodes in propagation cavity of p modes, and n_g the number of radial nodes in propagation cavity of g modes. The parameter $\beta_{\ell,n}$ measures the size of rotational splitting. Its general expression for a uniformly rotating star is described by Christensen-Dalsgaard (2003) as

$$\beta_{\ell,n} = \frac{\int_0^R (\xi_r^2 + L^2 \xi_h^2 - 2\xi_r \xi_h - \xi_h^2) r^2 \rho dr}{\int_0^R (\xi_r^2 + L^2 \xi_h^2) r^2 \rho dr}, \quad (4)$$

where $L^2 = \ell(\ell + 1)$, ρ the local density, ξ_r and ξ_h being the radial displacement and the horizontal displacement, respectively. For high-order g modes, $\beta_{\ell,n}$ can be simplified into $1 - \frac{1}{\ell(\ell+1)}$, which is in accordance with the term in Equation (1). In Figure 3, we show the theoretical values of $\beta_{\ell,n}$ for theoretical oscillation frequencies. As shown in the figure, most of $\beta_{\ell,n}$ are in accordance with the asymptotic value 0.5 for $\ell = 1$ modes and 0.833 for $\ell = 2$ modes. They show more pronounced g-mode characters in the star. Meanwhile, it can be found that $\beta_{\ell,n}$ of several oscillation modes clearly deviate from the asymptotic value. They show more pronounced p-mode characters in the star.

In Table 3, we show comparisons of the theoretical frequencies and the observed frequencies. The theoretical frequencies with $m \neq 0$ are deduced from $m = 0$ modes in Table 2 on basis of the parameter $\beta_{\ell,n}$. It can be seen in Table 3 that $m = 0$ components in Multiplet 1, 2, 3, 4, 6, and 10 are detected. However, $m = 0$ components in Multiplet 5, 7, 8, 9, 11, 12,

13, 14, and 15 have not been detected. The filled circles in Figure 3 mark $m = 0$ components in these multiplets of Table 3. As shown in Figure 3, the values of $\beta_{\ell,n}$ for oscillation modes with $m = 0$ in Multiplet 1, 2, 3, 4, 6, and 10 show a good agreement with the asymptotic value of g modes. For Multiplet 7, 8, 9, 11, 12, 13, 14, and 15, the values of $\beta_{\ell,n}$ of their corresponding $m = 0$ modes also agree well with the asymptotic value. The above analyses also show that performing mode identifications on basis of the regularities of g modes is self-consistent.

Furthermore, we give possible mode identifications for f_{12} , f_{13} , and f_{23} , and list them in Table 4. For f_{12} , we find that the frequency (1, 4, -23, +1) 127.447 μHz may be its possible model counterpart. Moreover, we notice in Table 4 that both of (2, 2, -61, +2) 94.290 μHz and (2, 2, -57, +1) 94.370 μHz are possible model counterparts for f_{23} . As discussed in Section 2, the spherical harmonic degree of f_{15} allows of two possibilities, i.e., $\ell = 1$ or $\ell = 2$. For the former case, f_5 and f_{15} constitute one incomplete triplet (Multiplet 5 in Table 1). It can be seen in Table 3 that (1, 0, -50, -1) 54.580 μHz and (1, 0, -50, +1) 62.534 μHz perhaps are their model counterparts. For this case, we notice in Figure 3 that $\beta_{\ell,n}$ of the $m \neq 0$ component (1, 0, -50, 0) 58.557 μHz clearly deviated from the asymptotic value 0.5. For the latter case, f_{13} and f_{15} constitute one incomplete quintuplet, and (2, 0, -102, -2) 40.236 μHz and (2, 0, -102, +2) 61.238 μHz may be their mode counterparts. For this case, $\beta_{\ell,n}$ of the central component (2, 0, -102, 0) 50.737 μHz is 0.833, which agrees well with the asymptotic value.

4.2. Discussions

When we do model fittings, we only use the fundamental radial mode f_1 , and two nonradial oscillation modes f_{11} and f_{32} to fit with theoretical calculated frequencies. Figure 4 illustrates the profiles of Brunt-Väisälä frequency N and Lamb frequency L_{ℓ} ($\ell = 1, 2$) for the best-fitting model. Figure 5 illustrates the scaled radial displacement eigenfunctions for the fundamental radial mode f_1 and two nonradial oscillation modes f_{11} and f_{32} . We adopt the default boundary of the helium core of MESA, and mark the position of the hydrogen fraction $X_{\text{cb}} = 0.01$ in Figures 4 and 5 with the vertical lines. The outer zone is the envelope of the star, and the inner zone is the helium core. It can be found in Figure 5 that the fundamental radial mode f_1 mainly propagates in the stellar envelope, and then characterizes the features of the stellar envelope. However for the two nonradial oscillation modes f_{11} and f_{32} , they have pronounced features of mixed modes. Namely, distinct g-mode features appear in the helium core and p-mode features appear in the stellar envelope. Thus the two nonradial oscillation modes can characterize the features of the helium core.

To investigate more detailed information on the structure of EE Cam, we introduce two asteroseismic quantities, the acoustic radius τ_0 and the period separation Π_0 . Both of τ_0 and Π_0 are independent of ℓ . The acoustic radius τ_0 is the sound travel time for a sound wave from the core of the star to the surface. Aerts et al. (2010) define the acoustic radius τ_0 as

$$\tau_0 = \int_0^R \frac{dr}{c_s}, \quad (5)$$

where c_s denotes the adiabatic sound speed. The value of c_s inside the helium core is much larger than that inside the stellar envelope, thus the features of the envelope of the star

can be characterized by the acoustic radius τ_0 . The expression of Π_0 is described as

$$\Pi_0 = 2\pi^2 \left(\int_0^R \frac{N}{r} dr \right)^{-1} \quad (6)$$

(Unno et al. 1979; Tassoul 1980; Aerts et al. 2010). In Equation (6), N denotes the Brunt–Väisälä frequency. The period separation Π_0 is dominated by the behavior of Brunt–Väisälä frequency inside the helium core of the star. Then the features of the helium core of the star can be characterized by Π_0 .

According to the analyses of Chen et al. (2016), both of the stellar envelope and the helium core need to match the actual structure of EE Cam, in order to fit the three pulsation modes (f_1 , f_{11} , and f_{32}). In Figure 2, it is very evident that $1/\chi^2$ of theoretical model with $Z = 0.028$ and $M = 2.04$ is much higher than those of other theoretical models. Hence τ_0 and Π_0 are determined to be 5.80 hr and 463.7 s, respectively. The size of the helium core of EE Cam is estimated to be about $M_{\text{He}} = 0.181 M_{\odot}$ and $R_{\text{He}} = 0.0796 R_{\odot}$.

In addition, the rotational period P_{rot} of EE Cam is determined to be $1.84^{+0.07}_{-0.05}$ days. The theoretical radius R of the best-fitting model is $4.12 R_{\odot}$. According to the formula $v_{\text{rot}} = 2\pi R/P_{\text{rot}}$, the equatorial rotation velocity v_{rot} is estimated to be $113.6^{+2.7}_{-4.1}$ km s $^{-1}$. Based on the inclination angle $i = 34 \pm 4$ deg (Breger et al. 2015), the value of $v_{\text{rot}} \sin i$ is deduced to be $63.5^{+7.8}_{-8.7}$ km s $^{-1}$, which is in accordance with the value $v \sin i = 51 \pm 8$ km s $^{-1}$ of Bush & Hintz (2008) and slight higher than the value $v \sin i = 40 \pm 3$ km s $^{-1}$ of Breger et al. (2007).

The δ Scuti star EE Cam is an evolved star. It can be noticed in Table 2 that the frequency spectrum of EE Cam is very dense. The effects of rotational splitting will make the frequency spectrum much more complicated. Dziembowski et al. (1993) analyzed the effects of rotation on the frequency spectra of SPB stars and found that the rotationally split multiplets already begin to overlap at a rotational velocity of about few km s $^{-1}$. We searched for frequency differences ranging from 1 μ Hz to 30 μ Hz in the observed frequencies of EE Cam. If oscillation modes with $\ell = 3$ are considered, we also found another possible scheme of mode identifications. There are fourteen sets of rotationally split multiplets, including three sets of multiplets with $\ell = 1$ (i.e., (f_{22}, f_8, f_9) , (f_6, f_{15}) , and (f_{27}, f_{31})), seven sets of multiplets with $\ell = 2$ (i.e., (f_{19}, f_{21}, f_3) , (f_{10}, f_{28}, f_{33}) , (f_{32}, f_{12}) , (f_{11}, f_{34}) , (f_{13}, f_5) , (f_{16}, f_{20}) , (f_{25}, f_{35})), and four sets of multiplets with $\ell = 3$ (i.e., (f_{23}, f_{24}, f_{30}) , (f_{18}, f_7) , (f_{14}, f_{17}) , (f_{37}, f_{39})). Four observed frequencies (i.e., f_2 , f_4 , f_{36} , and f_{38}) do not show frequency splitting. In this case, we found that most of frequency differences in those multiplets are two or more times that of the averaged rotational splittings. Besides, the dipole mode f_2 identified by Breger et al. (2015) does not show frequency splittings. The frequency f_3 is identified as a mode with $\ell = 2$ on basis of the regularities of rotational splitting. However, Breger et al. (2015) suggested that f_3 is a dipole mode based on the line-profile variations. As a consequence, we suggest the mode identifications in Section 2 in our work.

In our work, we fit three frequencies (f_1 , f_{11} , and f_{32}) for each stellar model by changing three independent physical parameters, i.e., the stellar mass M , the metallicity Z , and the effective temperature T_{eff} . To test effects of other physical parameters like the convective core overshooting on our fit-

ting results, much more stellar models have been computed, f_{ov} ranging from 0.001 to 0.010 with a step of 0.001. The parameter of f_{ov} describes the efficiency of the overshooting mixing, and the definition of f_{ov} is identical to that of Chen et al. (2017). After doing model fittings, we find 13 other stellar models fitting well to the three frequencies (f_1 , f_{11} , and f_{32}). Then we compare their theoretical frequencies with the observed frequencies in Table 3. Among these 13 stellar models, the structures of two stellar models with $(M, Z, f_{\text{ov}}, \chi^2) = (2.03, 0.026, 0.001, 0.0065)$ and $(2.01, 0.025, 0.002, 0.0079)$ are alike with that of our best-fitting model. Their acoustic radius τ_0 and period separation Π_0 are (5.82 hr, 463.5 s) and (5.79 hr, 463.8 s) respectively. They can reproduce the multiplets in Table 3. However, their values of χ^2 are higher than that of our best-fitting model one order of magnitude. The other 11 stellar models can not reproduce all of those multiplets in Table 3.

5. SUMMARY AND CONCLUSIONS

In this work, we have performed a detailed asteroseismic analysis for the δ Scuti pulsating star EE Cam. We try to disentangle the observed frequency spectra of EE Cam with the method of the rotational splitting. Then we build a grid of theoretical models to fitting the identified oscillation modes, aiming at reproducing these observed multiplets and getting the accurate fundamental stellar parameters, as well as investigating the information on the structure of the pulsating star. The main results obtained are summarized as follows.

1. The frequency spectra of the δ Scuti pulsating star EE Cam can be disentangled only with oscillation modes of $\ell = 0, 1$, and 2. A total of fifteen sets of multiplets are found, including five sets of $\ell = 1$ multiplets and ten sets of $\ell = 2$ multiplets. The rotational period P_{rot} is deduced to be $1.84^{+0.07}_{-0.05}$ days from the frequency differences in these multiplets.

2. According to the results of model fittings, we select the theoretical model with the minimum value of χ^2 as the best-fitting model, which has $M = 2.04 M_{\odot}$, $Z = 0.028$, $T_{\text{eff}} = 6433$ K, $\log L/L_{\odot} = 1.416$, $R = 4.12 R_{\odot}$, $\log g = 3.518$, and $\chi^2 = 0.00035$. For the best-fitting model, the observed multiplets are well matched.

3. Based on the best-fitting model, we find that most of the oscillation frequencies belong to the so-called mixed modes. The fundamental radial mode f_1 mainly offers constraints on the properties of the stellar envelope, and these properties can be characterized by the acoustic radius τ_0 . However for the two nonradial oscillation modes f_{11} and f_{32} , they mainly offer constraints on the helium core, for which the features can be characterized by the period separation Π_0 . Finally, τ_0 and Π_0 are determined to be 5.80 hr and 463.7 s respectively, and the size of the helium core is estimated to be $M_{\text{He}} = 0.181 M_{\odot}$ and $R_{\text{He}} = 0.0796 R_{\odot}$.

This work is supported by the NSFC of China (Grant No. 11333006, 11521303, and 11503079) and by the foundation of Chinese Academy of Sciences (Grant No. XDB09010202). The authors gratefully acknowledge an anonymous referee for instructive advice and productive suggestions. The authors gratefully acknowledge the computing time granted by the Yunnan Observatories, and provided on the facilities at the Yunnan Observatories Supercomputing Platform. The authors also acknowledge the discussions with J.-J. Guo, Q.-S. Zhang, T. Wu, G.-F. Lin.

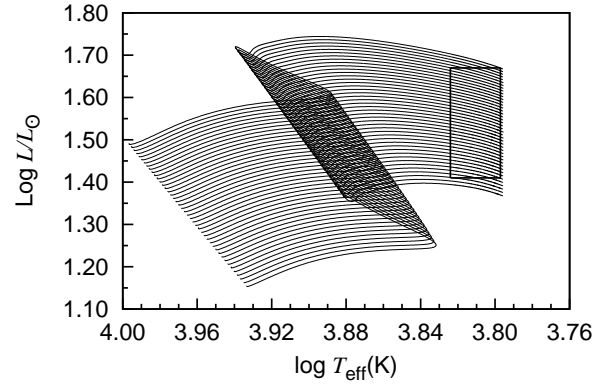


FIG. 1.— Evolutionary tracks. The rectangle marks the 1σ error box of the observed parameters, $1.41 < \log L/L_{\odot} < 1.67$ and $6269 \text{ K} < T_{\text{eff}} < 6669 \text{ K}$.

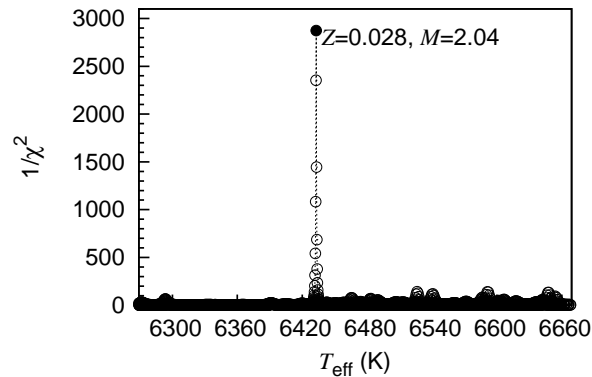


FIG. 2.— Plot of $1/\chi^2$ against the effective temperature T_{eff} of all grid models falling in the error box. The filled circle marks the best-fitting model.

REFERENCES

- Aerts, C., Christensen-Dalsgaard, J., & Kurtz, D. W. 2010, *Asteroseismology* (Berlin, Heidelberg: Springer)
- Ammons, S. M., Robinson, S. E., Strader, J., et al. 2006, *ApJ*, 638, 1004
- Aizenman, M., Smeyers, P., & Weigert, A. 1977, *A&A*, 58, 41
- Balona, L. A. 2014, *MNRAS*, 439, 3453
- Böhm-Vitense, E. 1958, *Z. Astrophys.*, 46, 108
- Breger, M., & Hiesberger, F. 1999, *A&AS*, 135, 547
- Breger, M., Rucinski, S. M., & Reegen, P. 2007, *AJ*, 134, 1994
- Breger, M., Lenz, P., Pamyatnykh, A. A., Schmid, V. S., & Beck, P. G. 2015, *A&A*, 575, A46
- Brickhill, A. J. 1975, *MNRAS*, 170, 405
- Bush, T. C., & Hintz, E. G. 2008, *AJ*, 136, 1061
- Chen, X. H., Li, Y., Lai, X. J., & Wu, T. 2016, *A&A*, 593, A69
- Chen, X. H., Li, Y., Lin, G. F., Chen, Y. H., & Guo, J. J. 2017, *ApJ*, 834, 146
- Christensen-Dalsgaard, J. 2003, *Lecture Notes on Stellar Oscillations*, Fifth Edition, available at <http://astro.phys.au.dk/~jcd/oscilnotes/>
- Christensen-Dalsgaard, J. 2008, *Ap&SS*, 316, 113
- Dziembowski, W. A., Moskalik, P., & Pamyatnykh, A. A. 1993, *MNRAS*, 265, 588
- Dotter, A., Chaboyer, B., Jevremović, D., et al. 2008, *ApJS*, 178, 89-101
- García Hernández, A., Moya, A., Michel, E., et al. 2013, *A&A*, 559, A63
- Granzer, T., Reegen, P., & Strassmeier, K. G. 2001, *Astronomische Nachrichten*, 322, 325
- Grevesse, N., & Sauval, A. J. 1998, *Space Sci. Rev.*, 85, 161
- Koen, C. 2001, *MNRAS*, 321, 44
- Lignières, F., Rieutord, M., & Reese, D. 2006, *A&A*, 455, 607
- Nordström, B., Mayor, M., Andersen, J., et al. 2004, *A&A*, 418, 989
- Olsen, E. H. 1980, *A&AS*, 39, 205
- Paparo, M., Bognár, Z., Benkő, J. M., et al. 2013, *A&A*, 557, A27
- Paxton, B., Bildsten, L., Dotter, A., et al. 2011, *ApJS*, 192, 3
- Paxton, B., Cantiello, M., Arras, P., et al. 2013, *ApJS*, 208, 4
- Perryman, M. A. C., Lindegren, L., Kovalevsky, J., et al. 1997, *A&A*, 323, L49
- Poretti, E., Michel, E., Garrido, R., et al. 2009, *A&A*, 506, 85
- Strassmeier, K. G., Boyd, L. J., Epanand, D. H., & Granzer, T. 1997, *PASP*, 109, 697
- Tassoul, M. 1980, *ApJS*, 43, 469
- Thompson, B., Frinchaboy, P., Kinemuchi, K., Sarajedini, A., & Cohen, R. 2014, *AJ*, 148, 85
- Unno, W., Osaki, Y., Ando, H., & Shibahashi, H. 1979, *Nonradial Oscillations of Stars* (Tokyo: Univ. Tokyo Press), 330
- van Leeuwen, F. 2007, *A&A*, 474, 653
- Winget, D. E., Nather, R. E., Clemens, J. C., et al. 1991, *ApJ*, 378, 326

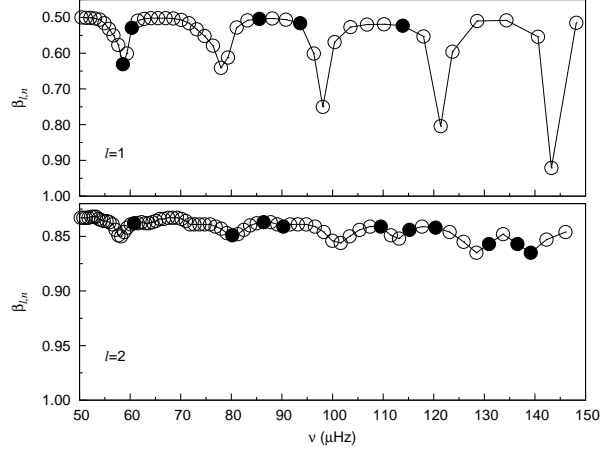


FIG. 3.— Plot of $\beta_{\ell,n}$ against the theoretical frequency ν of the best-fitting model. The filled circles mark $m = 0$ modes of the multiplets in Table 3.

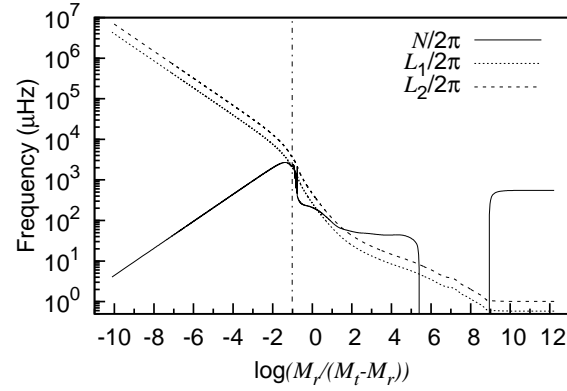


FIG. 4.— N shows Brunt–Väisälä frequency and L_ℓ ($\ell = 1, 2$) show Lamb frequency. M_t shows the stellar mass. The vertical line marks the boundary of the helium core.

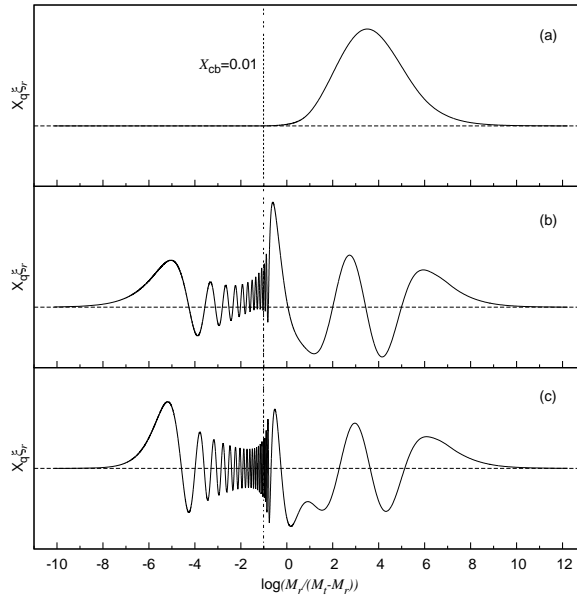


FIG. 5.— Scaled radial displacement eigenfunctions for the fundamental radial mode f_1 and the two nonradial oscillation modes f_{11} and f_{32} for the best-fitting model. $X_q = \sqrt{q(1-q)}$ and $q = M_r/M_t$. Panel (a) is for the fundamental radial mode $57.123 \mu\text{Hz}$ ($\ell = 0, n_p = 0, n_g = 0$). Panel (b) is for the oscillation mode $113.868 \mu\text{Hz}$ ($\ell = 1, n_p = 3, n_g = -25$). Panel (c) is for the oscillation mode $120.369 \mu\text{Hz}$ ($\ell = 2, n_p = 3, n_g = -41$). Vertical line marks the boundary of the helium core.

TABLE 1
 POSSIBLE ROTATIONAL SPLITS FOUND IN OBSERVED FREQUENCIES. THE SERIAL NUMBERS OF THE OBSERVED FREQUENCIES IN BREGER ET AL. (2015) ARE ADOPTED. FREQ. IS THE OBSERVED FREQUENCIES IN UNIT OF μHz , AND $\delta\nu$ THE FREQUENCY DIFFERENCE IN UNIT OF μHz

Multiplet	ID	Freq. (μHz)	$\delta\nu$ (μHz)	l	m	Multiplet	ID	Freq. (μHz)	$\delta\nu$ (μHz)	l	m
1	f_{25}	110.510	3.376	1	-1	8	f_{36}	127.547	5.257	2	(-2, -1, 0, +1)
	f_{11}	113.886		1	0		f_{38}	132.804		2	(-1, 0, +1, +2)
	f_{28}	117.063	3.177	1	+1		9	f_{30}	119.420	5.242	2
2	f_6	57.147	3.198	1	(-1, 0)	f_{33}		124.662	2		(-1, 0, +1, +2)
	f_2	60.345		1	(0, +1)	10		f_{27}	115.266	10.600	2
3	f_{20}	85.341	3.378	1	(-1, 0)		f_{35}	125.866	2		(0, +1, +2)
	f_{21}	88.719		1	(0, +1)		11	f_{18}	79.056	16.608	2
4	f_{22}	93.218	3.227	1	(-1, 0)	f_8		95.664	2		(+1, +2)
	f_3	96.445		1	(0, +1)	12		f_{19}	81.195	16.674	2
5	f_5	55.144	6.438	1	-1		f_9	97.869	2		(+1, +2)
	f_{15}	61.582		1	+1		13	f_{16}	69.725	21.775	2
6	f_{10}	109.677	10.677	2	-2	f_7		91.500	2		+2
	f_{32}	120.354		2	0	14		f_{24}	98.519	21.188	2
	f_{37}	131.031		2	+2		f_{31}	119.707	2		+2
7	f_4	50.001	5.309	2	-2	15	f_{34}	125.531	21.591	2	-2
	f_{14}	55.310		2	-1		f_{39}	147.122		2	+2
	f_{17}	71.803		16.493	2		+2				

TABLE 2

THEORETICAL FREQUENCIES DERIVED FROM THE BEST-FITTING MODEL. ν_{theo} IS THE CALCULATED FREQUENCY IN UNIT OF μHz . n_p DENOTES THE NUMBER OF RADIAL NODES IN PROPAGATION CAVITY OF P-MODE. n_g DENOTES THE NUMBER OF RADIAL NODES IN PROPAGATION CAVITY OF G-MODE. $\beta_{\ell,n}$ IS ONE PARAMETER MEASURING THE SIZE OF ROTATIONAL SPLITTING.

$\nu_{\text{theo}}(\ell, n_p, n_g)$ (μHz)	$\beta_{\ell,n}$	$\nu_{\text{theo}}(\ell, n_p, n_g)$ (μHz)	$\beta_{\ell,n}$	$\nu_{\text{theo}}(\ell, n_p, n_g)$ (μHz)	$\beta_{\ell,n}$	$\nu_{\text{theo}}(\ell, n_p, n_g)$ (μHz)	$\beta_{\ell,n}$
57.123(0, 0, 0)		62.767(1, 1, -47)	0.504	35.313(2, 0, -148)	0.834	58.223(2, 0, -88)	0.850
74.986(0, 1, 0)		64.110(1, 1, -46)	0.502	35.553(2, 0, -147)	0.834	58.806(2, 0, -87)	0.846
95.185(0, 2, 0)		65.526(1, 1, -45)	0.502	35.765(2, 0, -146)	0.835	59.437(2, 0, -86)	0.842
116.820(0, 3, 0)		67.006(1, 1, -44)	0.502	35.952(2, 0, -145)	0.835	60.104(2, 0, -85)	0.839
138.568(0, 4, 0)		68.537(1, 1, -43)	0.503	36.169(2, 0, -144)	0.834	60.795(2, 0, -84)	0.838
		70.094(1, 1, -42)	0.507	36.415(2, 0, -143)	0.834	61.505(2, 1, -84)	0.838
30.091(1, 0, -100)	0.500	71.639(1, 1, -41)	0.516	36.674(2, 0, -142)	0.834	62.228(2, 1, -83)	0.837
30.403(1, 0, -99)	0.500	73.156(1, 1, -40)	0.533	36.943(2, 0, -141)	0.833	62.957(2, 1, -82)	0.838
30.720(1, 0, -98)	0.500	74.708(1, 1, -39)	0.552	37.219(2, 0, -140)	0.833	63.682(2, 1, -81)	0.838
31.041(1, 0, -97)	0.500	76.354(1, 1, -38)	0.579	37.499(2, 0, -139)	0.833	64.394(2, 1, -80)	0.837
31.368(1, 0, -96)	0.500	77.946(1, 1, -37)	0.641	37.783(2, 0, -138)	0.833	65.109(2, 1, -79)	0.836
31.700(1, 0, -95)	0.500	79.322(1, 2, -37)	0.612	38.069(2, 0, -137)	0.833	65.857(2, 1, -78)	0.834
32.034(1, 0, -94)	0.500	81.043(1, 2, -36)	0.528	38.358(2, 0, -136)	0.833	66.655(2, 1, -77)	0.834
32.363(1, 0, -93)	0.500	83.174(1, 2, -35)	0.508	38.646(2, 0, -135)	0.834	67.500(2, 1, -76)	0.833
32.685(1, 0, -92)	0.500	85.536(1, 2, -34)	0.504	38.928(2, 0, -134)	0.834	68.378(2, 1, -75)	0.833
33.014(1, 0, -91)	0.500	88.075(1, 2, -33)	0.503	39.190(2, 0, -133)	0.834	69.274(2, 1, -74)	0.833
33.362(1, 0, -90)	0.500	90.773(1, 2, -32)	0.506	39.436(2, 0, -132)	0.834	70.165(2, 1, -73)	0.834
33.727(1, 0, -89)	0.500	93.591(1, 2, -31)	0.516	39.699(2, 0, -131)	0.834	71.015(2, 1, -72)	0.836
34.107(1, 0, -88)	0.500	96.305(1, 2, -30)	0.601	39.989(2, 0, -130)	0.833	71.835(2, 1, -71)	0.839
34.499(1, 0, -87)	0.500	98.085(1, 2, -29)	0.750	40.299(2, 0, -129)	0.833	72.713(2, 1, -70)	0.839
34.902(1, 0, -86)	0.500	100.413(1, 3, -29)	0.569	40.621(2, 0, -128)	0.833	73.682(2, 1, -69)	0.839
35.315(1, 0, -85)	0.500	103.547(1, 3, -28)	0.527	40.953(2, 0, -127)	0.833	74.712(2, 1, -68)	0.839
35.738(1, 0, -84)	0.500	106.822(1, 3, -27)	0.520	41.293(2, 0, -126)	0.833	75.780(2, 1, -67)	0.839
36.171(1, 0, -83)	0.500	110.184(1, 3, -26)	0.519	41.639(2, 0, -125)	0.833	76.874(2, 1, -66)	0.841
36.611(1, 0, -82)	0.500	113.868(1, 3, -25)	0.523	41.989(2, 0, -124)	0.833	77.982(2, 1, -65)	0.843
37.058(1, 0, -81)	0.499	117.968(1, 3, -24)	0.553	42.338(2, 0, -123)	0.833	79.089(2, 1, -64)	0.847
37.507(1, 0, -80)	0.499	121.376(1, 3, -23)	0.804	42.684(2, 0, -122)	0.833	80.185(2, 1, -63)	0.849
37.958(1, 0, -79)	0.499	123.691(1, 4, -23)	0.596	43.021(2, 0, -121)	0.833	81.290(2, 1, -62)	0.848
38.409(1, 0, -78)	0.499	128.581(1, 4, -22)	0.511	43.343(2, 0, -120)	0.833	82.454(2, 2, -62)	0.844
38.870(1, 0, -77)	0.499	134.355(1, 4, -21)	0.508	43.649(2, 0, -119)	0.833	83.701(2, 2, -61)	0.840
39.353(1, 0, -76)	0.499	140.605(1, 4, -20)	0.554	43.974(2, 0, -118)	0.833	85.021(2, 2, -60)	0.838
39.864(1, 0, -75)	0.499	143.267(1, 4, -19)	0.921	44.337(2, 0, -117)	0.833	86.392(2, 2, -59)	0.837
40.400(1, 0, -74)	0.499	148.171(1, 5, -19)	0.515	44.726(2, 0, -116)	0.833	87.775(2, 2, -58)	0.837
40.958(1, 0, -73)	0.499			45.128(2, 0, -115)	0.833	89.082(2, 2, -57)	0.839
41.534(1, 0, -72)	0.499	30.084(2, 0, -174)	0.833	45.537(2, 0, -114)	0.833	90.280(2, 2, -56)	0.841
42.125(1, 0, -71)	0.499	30.264(2, 0, -173)	0.834	45.951(2, 0, -113)	0.833	91.607(2, 2, -55)	0.839
42.729(1, 0, -70)	0.499	30.438(2, 0, -172)	0.834	46.370(2, 0, -112)	0.833	93.140(2, 2, -54)	0.839
43.342(1, 0, -69)	0.499	30.570(2, 0, -171)	0.837	46.795(2, 0, -111)	0.833	94.796(2, 2, -53)	0.839
43.964(1, 0, -68)	0.499	30.693(2, 0, -170)	0.835	47.223(2, 0, -110)	0.833	96.521(2, 2, -52)	0.841
44.593(1, 0, -67)	0.499	30.870(2, 0, -169)	0.834	47.647(2, 0, -109)	0.832	98.262(2, 2, -51)	0.846
45.228(1, 0, -66)	0.499	31.062(2, 0, -168)	0.834	48.051(2, 0, -108)	0.831	99.951(2, 2, -50)	0.854
45.873(1, 0, -65)	0.499	31.257(2, 0, -167)	0.833	48.434(2, 0, -107)	0.830	101.599(2, 2, -49)	0.856
46.539(1, 0, -64)	0.499	31.452(2, 0, -166)	0.833	48.831(2, 0, -106)	0.831	103.365(2, 2, -48)	0.850
47.236(1, 0, -63)	0.499	31.651(2, 0, -165)	0.833	49.270(2, 0, -105)	0.832	105.315(2, 3, -48)	0.844
47.968(1, 0, -62)	0.499	31.855(2, 0, -164)	0.833	49.741(2, 0, -104)	0.832	107.396(2, 3, -47)	0.841
48.737(1, 0, -61)	0.500	32.065(2, 0, -163)	0.833	50.232(2, 0, -103)	0.833	109.533(2, 3, -46)	0.841
49.541(1, 0, -60)	0.500	32.278(2, 0, -162)	0.833	50.737(2, 0, -102)	0.833	111.514(2, 3, -45)	0.849
50.380(1, 0, -59)	0.500	32.492(2, 0, -161)	0.834	51.249(2, 0, -101)	0.833	113.148(2, 3, -44)	0.852
51.250(1, 0, -58)	0.501	32.702(2, 0, -160)	0.834	51.766(2, 0, -100)	0.833	115.191(2, 3, -43)	0.844
52.147(1, 0, -57)	0.501	32.895(2, 0, -159)	0.835	52.281(2, 0, -99)	0.832	117.683(2, 3, -42)	0.841
53.065(1, 0, -56)	0.503	33.041(2, 0, -158)	0.836	52.782(2, 0, -98)	0.832	120.369(2, 3, -41)	0.842
53.993(1, 0, -55)	0.506	33.203(2, 0, -157)	0.834	53.263(2, 0, -97)	0.832	123.145(2, 3, -40)	0.846
54.909(1, 0, -54)	0.516	33.412(2, 0, -156)	0.834	53.737(2, 0, -96)	0.834	125.894(2, 3, -39)	0.855
55.798(1, 0, -53)	0.532	33.635(2, 0, -155)	0.833	54.234(2, 0, -95)	0.835	128.436(2, 4, -39)	0.865
56.699(1, 0, -52)	0.550	33.865(2, 0, -154)	0.833	54.769(2, 0, -94)	0.836	130.908(2, 4, -38)	0.857
57.649(1, 0, -51)	0.577	34.099(2, 0, -153)	0.833	55.338(2, 0, -93)	0.836	133.694(2, 4, -37)	0.848
58.557(1, 0, -50)	0.631	34.335(2, 0, -152)	0.833	55.929(2, 0, -92)	0.837	136.539(2, 4, -36)	0.857
59.358(1, 1, -50)	0.601	34.575(2, 0, -151)	0.833	56.528(2, 0, -91)	0.839	139.175(2, 4, -35)	0.865
60.334(1, 1, -49)	0.529	34.819(2, 0, -150)	0.833	57.115(2, 0, -90)	0.844	142.286(2, 4, -34)	0.853
61.499(1, 1, -48)	0.509	35.066(2, 0, -149)	0.833	57.674(2, 0, -89)	0.849	146.036(2, 4, -33)	0.846

TABLE 3
COMPARISONS OF THE THEORETICAL FREQUENCIES AND THE OBSERVED MULTIPLETS OF TABLE 1. ν^{obs} IS THE OBSERVED FREQUENCIES IN UNIT OF μHz , ν^{theo} IS THE THEORETICAL FREQUENCIES IN UNIT OF μHz . $\Delta\nu = |\nu^{\text{obs}} - \nu^{\text{theo}}|$

Multiplet	ID	ν^{obs} (μHz)	$\nu^{\text{theo}}(\ell, m)$ (μHz)	$\Delta\nu$ (μHz)	Multiplet	ID	ν^{obs} (μHz)	$\nu^{\text{theo}}(\ell, m)$ (μHz)	$\Delta\nu$ (μHz)
1	f_{25}	110.510	110.571(1,-1)	0.061	8	f_{36}	127.547	128.271(2,-2)	0.724
	f_{11}	113.886	113.868(1,0)	0.018		f_{38}	132.804	133.723(2,-1)	0.919
	f_{28}	117.063	117.164(1,+1)	0.101		9	f_{30}	119.420	120.104(2,-2)
2	f_6	57.147	56.999(1,-1)	0.148	f_{33}		124.662	125.506(2,-1)	0.844
	f_2	60.345	60.334(1,0)	0.011	10	f_{27}	115.266	115.191(2,0)	0.075
3	f_{20}	85.341	85.536(1,0)	0.195		f_{35}	125.866	125.830(2,+2)	0.036
	f_{21}	88.719	88.712(1,+1)	0.007	11	f_{18}	79.056	79.678(2,-2)	0.622
4	f_{22}	93.218	93.591(1,0)	0.373		f_8	95.664	95.581(2,+1)	0.083
	f_3	96.445	96.843(1,+1)	0.398	12	f_{19}	81.195	81.117(2,-1)	0.078
5	f_5	55.144	54.580(1,-1)	0.564		f_9	97.869	96.943(2,+2)	0.926
	f_{15}	61.582	62.534(1,+1)	0.952	13	f_{16}	69.725	69.482(2,-2)	0.243
6	f_{10}	109.677	109.755(2,-2)	0.078		f_7	91.500	90.887(2,+2)	0.613
	f_{32}	120.354	120.369(2,0)	0.015	14	f_{24}	98.519	98.931(2,-2)	0.412
	f_{37}	131.031	130.983(2,+2)	0.048		f_{31}	119.707	120.134(2,+2)	0.427
7	f_4	50.001	50.231(2,-2)	0.230	15	f_{34}	125.531	125.736(2,-2)	0.205
	f_{14}	55.310	55.513(2,-1)	0.203		f_{39}	147.122	147.342(2,+2)	0.220
	f_{17}	71.803	71.359(2,+2)	0.444					

TABLE 4
POSSIBLE MODE IDENTIFICATIONS FOR THE THREE ISOLATED PULSATION FREQUENCIES ON BASIS OF THE BEST-FITTING MODEL. $\Delta\nu = |\nu^{\text{obs}} - \nu^{\text{theo}}|$.

ID	ν^{obs} (μHz)	$\nu^{\text{theo}}(\ell, n_p, n_g, m)$ (μHz)	$\Delta\nu$ (μHz)
f_1	57.101	57.123(0,0,0)	0.022
f_{12}	127.707	127.447(1,4,-23,+1)	0.260
f_{13}	39.893	39.864(1,0,-75,0)	0.029
		39.825(2,0,-151,+1)	0.068
		39.989(2,0,-130,0)	0.096
		39.878(2,0,-115,-1)	0.015
f_{23}	94.319	94.290(2,2,-61,+2)	0.029
		94.370(2,2,-57,+1)	0.051